International Journal of Adhesion & Adhesives 130 (2024) 103602

Contents lists available at ScienceDirect

International Journal of Adhesion and Adhesives

journal homepage: www.elsevier.com/locate/ijadhadh

Harnessing the synergy of grout and adhesive: Numerical prediction of load capacity in hybrid composite joints

Sebastian Myslicki [a,*], Till Vallée [a], Marvin Kaufmann [a], Thomas Ummenhofer [b], Jakob Boretzki [b], Matthias Albiez [b]

[a] Fraunhofer Institute for Manufacturing Technology and Advanced Materials IFAM, Wiener Str. 12, 28 359, Bremen, Germany
[b] KIT Stahl- und Leichtbau, Versuchsanstalt für Stahl, Holz und Steine, Karlsruhe Institute of Technology, Otto-Ammann-Platz 1, 76 131, Karlsruhe, Germany

ARTICLE INFO

Keywords:
Epoxies
Steels
Destructive testing
Finite element stress analysis
Joint design
Mechanical properties of adhesives
Hybrid joints

ABSTRACT

This study examines grouted joints for offshore wind turbine systems, where gaps between steel pipes are filled with grout, relying on adhesion, friction and compression struts formed by shear keys. Concerns about the limited load carrying capacity of large diameter grouted joints in offshore structures have prompted investigation. Whilst adhesive bonds are recognized for load transfer in structural steel, the complete replacement of grouting with bonding alone is proving impractical for large gaps in offshore structures, posing challenges in terms of cost and handling. To address these challenges, the study presents an innovative hybrid grouted joint for steel structures that combines grout and adhesive layers. This novel approach replaces traditional large shear keys with distributed micro-shear keys — small granules embedded in the grout material. Under axial loading, the hybrid joint demonstrates robust performance, with a maximum nominal shear stress on the inner pipe of 30.1 MPa and consistent load capacity across tests. Average shear strength is in line with, and occasionally exceeds, expectations. Notably, the hybrid joint shows resilience in different configurations and maintains a low coefficient of variation of 5.5%, indicating consistent performance. When the influence of the adhesive material on the hybrid joint is examined, the effect on the joint stiffness is minimal, despite variations in adhesive stiffness. Sikadur 370, which has a higher modulus of elasticity than DuploTEC, shows similar deformation curves in the elastic region, emphasizing the robustness of the joint. Differences in the maximum loads are attributed to the thickness of the adhesive layer and the lower modulus of DuploTEC, resulting in different shear strengths. The proposed hybrid joint offers a promising solution to improve the performance of conventional grouts and adhesives in offshore structures. The study also formulates a failure criterion, performs numerical stress analysis, and models the effect of geometric dimensions, eccentricity, and misalignment on load capacity. The methodology's accuracy in predicting load capacity, supported by numerical analysis and large-scale joint simulations, contributes to a comprehensive understanding of hybrid joint performance in engineering applications.

1. Introduction

The joining of circular hollow sections (CHS) in offshore structures often involves the use of grout material and welded shear keys. However, these traditional methods can lead to stress concentrations, fatigue cracks, and damage to the grouting mortar. To overcome these challenges, hybrid grout connections with organic adhesive interfaces have been proposed. This study aims to explore the potential of such connections. To understand the fundamentals of this research, it is important to examine the similarities and differences between grouting and adhesive bonding.

1.1. Grouted connections

Grouted connections play a crucial role in maintaining the structural integrity of offshore wind turbine systems [1]. These connections involve joining steel tubes using grout material to fill the gap between them. The inner tube, known as the pile, and the outer tube, referred to as the sleeve, are commonly used in this configuration. Grout serves as a cost-effective alternative to structural adhesives for larger gap widths, besides allowing for curing under adverse temperature and moisture conditions. Shear keys can be incorporated to enhance the mechanical

* Corresponding author.
E-mail addresses: sebastian.myslicki@ifam.fraunhofer.de (S. Myslicki), till.vallee@ifam.fraunhofer.de (T. Vallée), marvin.kaufmann@ifam.fraunhofer.de (M. Kaufmann), thomas.ummenhofer@kit.edu (T. Ummenhofer), jakob.boretzki@kit.edu (J. Boretzki), matthias.albiez@kit.edu (M. Albiez).

https://doi.org/10.1016/j.ijadhadh.2023.103602
Received 2 June 2023; Received in revised form 5 December 2023; Accepted 18 December 2023
Available online 10 January 2024

interlocking of the grout and increase the load-bearing capacity [2]. The load-bearing mechanism in these connections involves adhesion and friction between the grout and steel tubes, as well as compression struts formed by the shear keys [3]. Various factors influence the behaviour of grouted connections, including the diameter-to-thickness ratio of the tubes, the compressive strength of the grout, and the height-to-spacing ratio of the shear keys.

The performance of grouts depends on factors such as strength, durability, and process reliability. These factors include mix performance, ambient conditions, mixing and casting equipment, casting time, and early-stage thermal and mechanical loads. The aforesaid considerations are similar to those for structural adhesives and are crucial for ensuring the performance of grouted connections in challenging offshore conditions [4]. Design checks for grouted connections typically follow standards with empirical and analytical design equations. However, alternative mechanical models, such as non-linear finite element models and strut and tie models, have been employed to ensure mechanical consistency [5].

Billington et al. [6,7] conducted a comprehensive study on grouted joints, analysing the effects of surface compositions, grout material properties, and geometric factors. Based on 450 tests, they derived empirical relationships for the bond strength of grouted connections between tubular steel piles and pile sleeves. The bond strength depends on factors such as the radial stiffness of steel tubes and grout, length to diameter ratio of the connection, grout compressive strength, dimensions of mechanical shear keys, and surface roughness of the tubes. The bond strength is influenced by both frictional bond and mechanical shear keys, with the contribution from shear keys being proportional to the outstand-to-spacing ratio. Additionally, both contributions are proportional to the square root of grout compressive strength. A stiffness factor, denoted as K in Eq. (1), considers pile (subscript p), sleeve (s), and grout (g) stiffness, exhibiting a linear relationship with bond strength; with E being the Young's moduli, t thicknesses and D diameters.

$$K = \frac{E_g}{E_s}\frac{t_g}{D_g} + \left(\frac{D_s}{t_s} + \frac{D_p}{t_p}\right)^{-1} \tag{1}$$

Improving the frictional aspects of grouted joints is crucial for enhancing their performance. Failure modes of connections with shear keys include shear failure along the connectors when closely spaced and crushing of the grout on the stressed side of the shear keys with appropriate spacing, resulting in diagonal cracks in the grout [8]. However, there is a limit to the strength improvement of grouted joints, as the strength of the grout cannot be infinitely increased.

Lamport [9] developed a simplified analytical model to investigate various parameters in grouted connections. The results indicated that increasing the shear-key height or reducing the shear-key spacing might not necessarily result in a higher ultimate strength of the connection. This suggests that factors other than the geometric aspects of shear keys, such as the interaction between grout and steel, play a more significant role in determining the strength of the connection.

The ultimate strength equation for the connection, as specified by Krahl [10], considers two terms: the adhesion and friction strength between the pile and grout, and the confined strength of the grout multiplied by the ratio of the shear key's height to its spacing. Enhancements in the frictional aspects can have a significant impact on the performance of the connection, even when shear keys are used. The bond strength, typically ranging between 1 and 3 MPa (cf. [10] and Fig. 1), plays a crucial role in this improvement. It is worth noting that these bond strength values are relatively low compared to typical values achieved with structural adhesives [11–16], which are 5 to 10 times higher. Additionally, there is significant variability in bond strength values; this variability directly affects the corresponding design values (usually taken as means minus multiples of the standard deviation). Improving bond strengths would not only increase the average value but also reduce the scatter, leading to more reliable and consistent performance of grouted joints.

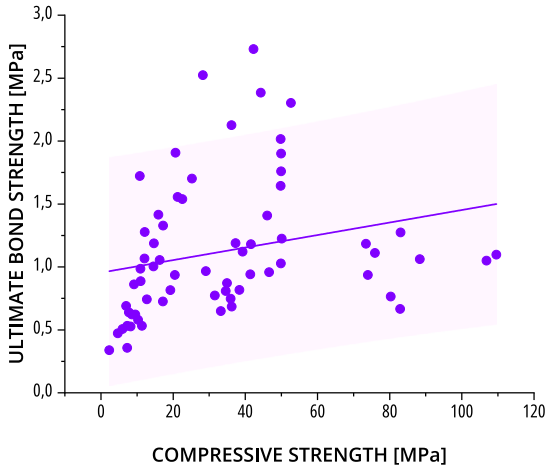

Fig. 1. Relationship between bond strength and compressive strength of the grout for plain pipes (redrawn with data from [10]); note the relatively low values of the ultimate bond strength, if compared to lap shear strength of usual structural adhesives.

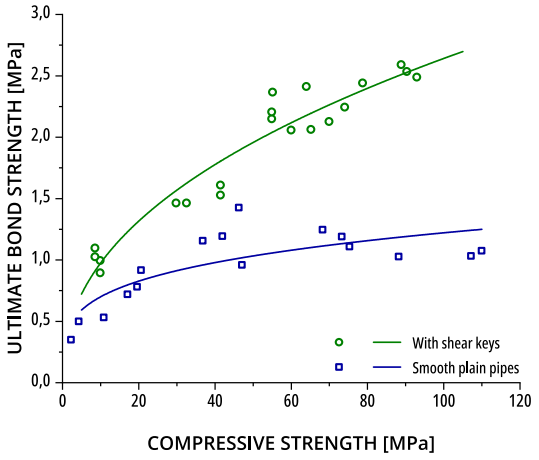

Fig. 2. Relationship between bond strength and compressive strength of the grout for a connection with shear keys and for plain pipe (redrawn with data from [7]); note the relatively low values of the ultimate bond strength, if compared to lap shear strength of usual structural adhesives.

Concerns regarding large-diameter grouted connections have been highlighted in previous studies, particularly with regards to design codes, testing conditions, and the steel-grout interface [8]. Issues such as lower coefficients of friction due to water penetration and susceptibility to crushing under repeated fatigue loads have raised concerns about the performance of the steel-grout interface. Fatigue assessments of grouted connections have primarily focused on vertical slippage caused by underestimating the cyclic effects on axial capacity [17]. Finite element simulations have demonstrated the gradual misalignment of grouted connections in structures subjected to fatigue, along with the negative influence of mechanical interlock on the performance [18]. The insufficient fatigue performance of mechanical shear keys often requires careful dimensioning and design approaches.

In summary, grout connections on smooth steel surfaces have limited load-bearing capacity due to the loss of adhesion between the grout and steel, compared to connections with shear keys, as illustrated in Fig. 2. Shear keys significantly increase the load-bearing capacity but can cause detachment of the mortar layer from the steel, especially under repeated loading below the water surface. Addressing this

detachment requires complex reinforcement measures to optimize the grout's load-bearing capacity.

1.2. Adhesively bonded connections

For structural steel, traditional joining methods like bolting and welding have long been favoured. Recent studies have highlighted the limited adoption of adhesives for load-bearing joints in structural steel. Examples include investigations on adhesively bonded steel tubes [11,12] and offshore structures [13,14] by Albiez et al. hybrid joints incorporating pre-tensioned bolts by Denkert et Vallée [15,16] and [19,20] by Yokozeki et al. However, adhesive bonding is gaining recognition as a viable complement or even substitute, particularly for load transmission purposes. The strength of an adhesive bond is governed by the cohesive [21] and adhesive strength [22]. Cohesive strength refers to the inherent strength of the adhesive itself, influenced by factors such as adhesive type, curing conditions, and environmental factors like temperature during loading. On the other hand, adhesive strength primarily relies on the surface conditions of the materials being bonded, with the interpenetration of the adhesive and adherend playing a critical role. Achieving proper surface preparation techniques, such as degreasing, blasting, priming, or chemical etching, becomes essential, especially when dealing with metal and metal oxide surfaces [23]. For further in-depth insights into adhesive bonding, including aspects beyond the scope of this paper, readers are encouraged to refer to relevant reference works [24,25].

The strength prediction of adhesively bonded joints is still a challenging task, despite being investigated for almost a century using empirical [26], analytical [27], and numerical methods [28]. The currently most popular methods for designing adhesively bonded joints are Fracture Mechanics (FM [29]) and Cohesive Zone Modelling (CZM [30]). FM requires a very extensive experimental characterization [31] and CZM foots on computationally challenging numerical implementation of cohesive laws [32]; both FM and CZM significantly depend on the geometrical specifications of the joints. Although FM and CZM are powerful tools for predicting the strength of a wide range of designs, they create a disruption regarding classical mechanics and usual dimensioning schemes [33]. Furthermore, the numerical complexity of both methods makes them almost out of reach for the common practitioner. Even more advanced techniques, such as the eXtended Finite Element Method [34] or meshless methods [35], while increasingly approaching the true complexity of the matter, further alienate practitioners from applying them. The aforesaid is particular relevant in engineering, where design methods need to be reliable and simple. Simplicity enables practitioners to understand procedures, reduces errors, and saves time.

While FM and CZM dominate the design of adhesively bonded joints, probabilistic methods (PM) remain underrepresented, even though they offer a straightforward and dependable approach for predicting joint strength. PM extend classical mechanics by redefining stress and strength as probabilities of survival [36,37]. They offer practitioners a way to use classical mechanics they are already familiar with to predict joint capacity with accuracy, without the need for new test setups or methods. Numerous studies, recently compiled by Vallée et al. [38], demonstrated the relative ease of implementation (further discussed in Section 2.5) and effectiveness of PM in predicting the strength of adhesively bonded joints across a wide variety of materials and joint types.

1.3. Proposed novelty

Critical to offshore wind turbine systems, grouted joints fill the gap between steel tubes with grout, relying on adhesion, friction and compression struts formed by shear keys to support the load. Factors influencing the behaviour include tube diameter to thickness ratio, grout compressive strength and shear key dimensions. Previous studies, such as those by Billington et al. have established empirical relationships for bond strength. However, there are concerns about the limited load carrying capacity of large diameter grouted connections, particularly in relation to design codes, test conditions and the steel grout interface.

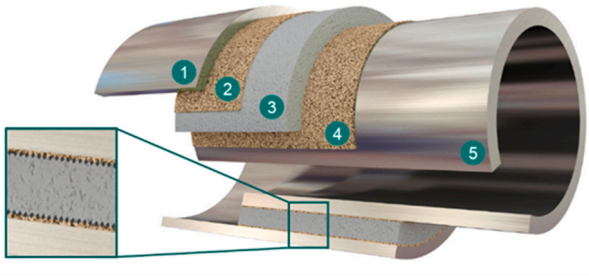

Fig. 3. Concept of a hybrid grout joint: (1) Outer tube (sleeve), (2) and (4) adhesive with integrated granulate, (3) grouting mortar, and (5) inner tube (pile).

Adhesive bonds, although less commonly used in structural steel, have gained recognition for load transfer purposes. The strength of an adhesive bond depends on the cohesive and adhesive strengths, which are influenced by factors such as the type of adhesive, curing conditions and surface preparation techniques. Completely replacing grouting with bonding alone is not a viable solution, mainly due to the large gaps between steel pipes in offshore structures. Bonding is effective for smaller gaps, but becomes impractical, expensive and difficult to handle for the large dimensions often encountered in these applications.

Grouted joints resemble adhesively bonded joints, where the grout's compressive strength represents cohesive strength and the conditions at the grout-steel interface define adhesive strength. Evaluating grouted joint strength involves calculating average shear strength based on failure load and interface surface area. However, the adhesion mechanisms differ between the sleeve and pile, and may described as friction (with the coefficient μ) augmented by a cohesive term (c) as $\tau = \sigma \times \mu + c$ [39]. Characterizing load transfer solely through shear stresses oversimplifies the interplay with transverse normal stresses.

This study presents an innovative hybrid grouted joint for steel structures that combines grout and adhesive layers. The novel design replaces conventional large shear keys with distributed micro-shear keys — small granules embedded in the grout material. This concept, similar to an almost continuous layer of very small shear keys within an organic adhesive, reduces stress concentrations and ensures a more uniform stress distribution. The proposed approach represents a promising solution to improve the performance of conventional grouts and adhesives in offshore structures, but has also potential application in bridge structures when it comes to connect large scale tubular elements—including to foundations.

The manuscript introduces the hybrid grouted joint for steel structures illustrated by Fig. 3. The joint's multilayer structure includes sandblasting, adhesive coating, and incorporation of inorganic granules for efficient load transfer and fatigue crack delay. Further details on development and validation were amply discussed in two previous publications [40,41].

1.4. Scope of this paper

The objective of this article is to develop, implement and validate a predictive framework for estimating the joint capacity of the grouted joints presented previously. This is achieved by employing numerical modelling to analyse the stress distribution within the joints, which is then combined to an experimentally determined failure criterion.

Due to the complexity of the subject, investigations were carried out on the materials, the interface and on joints. Alongside the experimental work, numerical modelling, with data based upon the characterization, was pursued, and compared to the test results for validations. The logic of the research is briefly summarized in Fig. 4.

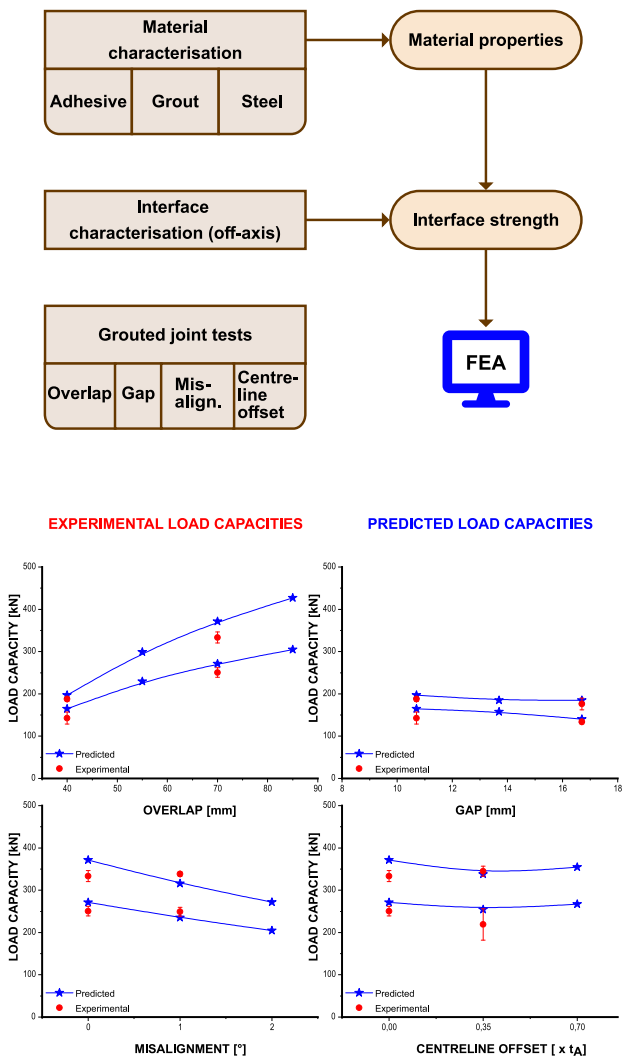

Fig. 4. Flowchart illustrating the experimental and numerical investigations reported in this paper.

2. Materials and methods

2.1. Materials

Two adhesives were identified based on their technical datasheets: Sikadur370 and DuploTEC 10490 SBF. Sikadur370, a two-component epoxy adhesive, was designed for bonding steel plates to concrete without a primer.

Both adhesives are qualified for structural and thermo-mechanical properties. Tensile strength and Young's modulus were determined according to EN DIN 527 at room temperature with a quasi-static loading rate of 1 mm/min. The specimen thickness was 3 mm for Sikadur370 and 0.1 mm for DuploTEC; the results are based on the average of 5 samples. Secondly, a lap shear test was carried out on 3 mm thick blasted S355 in accordance with DIN EN 1465 at a load rate of 5 mm/min at room temperature. Thick adhesion shear test (TAST) specimens were prepared and tested in accordance with DIN EN 14869-2 at room temperature with a loading rate of 0.5 mm/min and 5 replicates. The glass transition temperature (T_g) was determined on bulk samples after curing for at least 10 days at room temperature. The determination was made using Dynamic Mechanical Analysis (DMA) in a temperature range of −20 °C to 200 °C and a heating rate of 2 K/min. The results are summarized in Table 1.

Only one grout material, Pagel's HF10, was considered for evaluation. HF10 was chosen for its high flexural strength. Grout material testing followed DIN EN 196-1 standards, utilizing prism-shaped specimens measuring 40 mm × 40 mm × 160 mm. The testing involved a three-point bending test to measure bending strength, and compressive strength assessments were conducted on both halves of the specimens. The objective was to improve the mechanical interlocking mechanism by incorporating particles into the adhesive. Quartz sand was selected as the suitable filler due to its larger particle size and uniform distribution centred around 1 mm, enhancing particle fit within the adhesive. This resulted in improved mechanical interlocking and consistent performance. However, no additional properties of the particles were analysed beyond their size and distribution.

The study utilized hot rolled circular hollow sections (CHS) made according to EN 10025-1 from S355J2H steel. The material properties of the steel (yield strength 404.25 MPa, tensile strength 552.75 MPa, and Young's modulus E = 210 GPa) were assumed based on literature, and no specific characterization was conducted. Further information on the geometrical specifications, including diameters and thicknesses, can be found in subsequent sections.

All mechanical tests, including those for material characterization, characterization of the interface, and the hybrid joints, were carried out under laboratory conditions, i.e., at 23 °C and 50% rel. humidity.

2.2. Mechanical characterization of the interface

The strength of the adhesive–grout interface, including the effect of the granules embedded therein, was characterized about the simultaneous action of shear and normal (compressive and tensile) stress. For that, off-axis specimens were used; which load material or interfaces at an angle to its principal axis to evaluate strength and failure behaviour; for more details refer to [11,12,15,16]. The geometry of the off-axis samples, inspired by the specifications defined by DIN EN 12188:1999-07, is depicted in Fig. 5.

The specimens used in the experiments were made up of pairs of steel parts with a cross-sectional area of 15 × 30 mm^2, and off-axis angles of 0°, 30°, 45°, 60°, and 90°. Both Sikadur370 and DuploTEC were used in the tests featuring adhesively bonded interfaces. For the grouted interfaces, Pagel's HF10, Sikadur370, and DuploTEC, along with quartz sand, were applied in the same way as for the hybrid joints, with key steps described in Fig. 6. To allow for a moment-free introduction of the load, cardan joints were used during the tests, which were conducted at a load rate of 0.5 mm/min.

2.3. Hybrid joints

The manufacturing process of the hybrid grouted joint involved several steps, with the most important ones depicted in Fig. 7. Surface preparation of the steel was conducted by blasting with corundum to Sa 2½ level and degreasing with butanone (MEK). A 0.5 mm textile tape defined the lateral boundaries and thickness of the adhesive layers, shows Fig. 7a. After curing, the tape was removed, and wet adhesive was coated with quartz sand and pressed onto the steel surface, shown in both Fig. 7c to d.

Curing followed the manufacturer's guidelines, which for the DuploTEC meant curing at 130 °C. The joints were then grouted in an upright position, ensuring proper alignment using a fixture described in Fig. 7-right. The overlap length was set by placing the inner CHS on a circular pedestal, adjustable via a threaded rod within the outer CHS. The pedestal also acted as the bottom seal of the grout layer.

The grout was mixed according to the manufacturer's instructions and poured into the gap, as depicted in Fig. 7f. The self-levelling and self-compacting properties of the grout ensured adequate filling. To prevent shrinkage, the grout layer surface was kept moist and covered with a polyethylene film during the 28-day curing period.

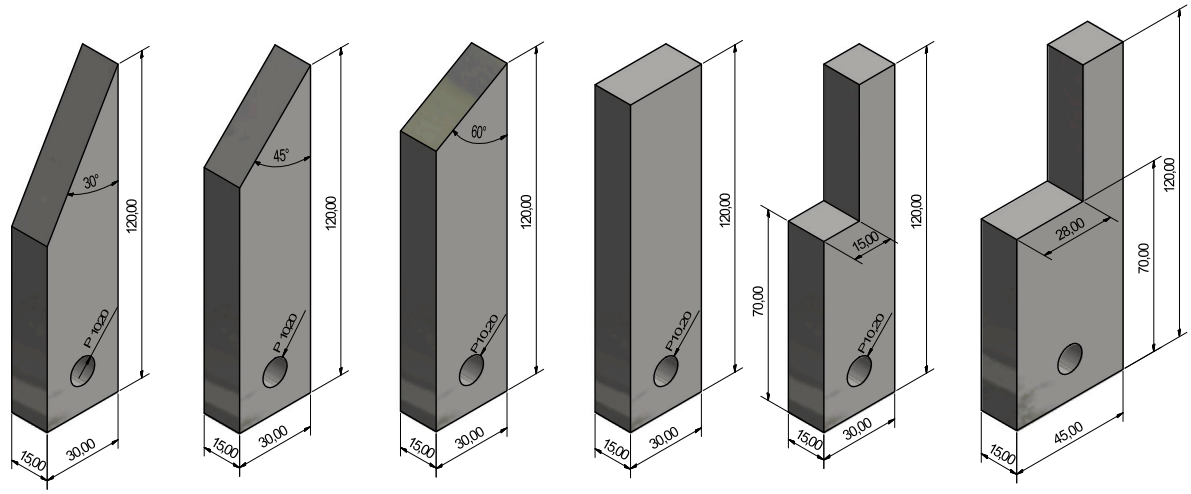

Fig. 5. Geometry of the off-axis samples to characterize the adhesive–grout interface (from top to down: off-axis angles of 0°, 30°, 45°, 60°, and 90°).

(a) Application of the adhesive (b) Application of the quartz sand (c) Cured adhesive-sand interface (d) Curing of the grout material

Fig. 6. Key steps in manufacturing the off-axis samples.

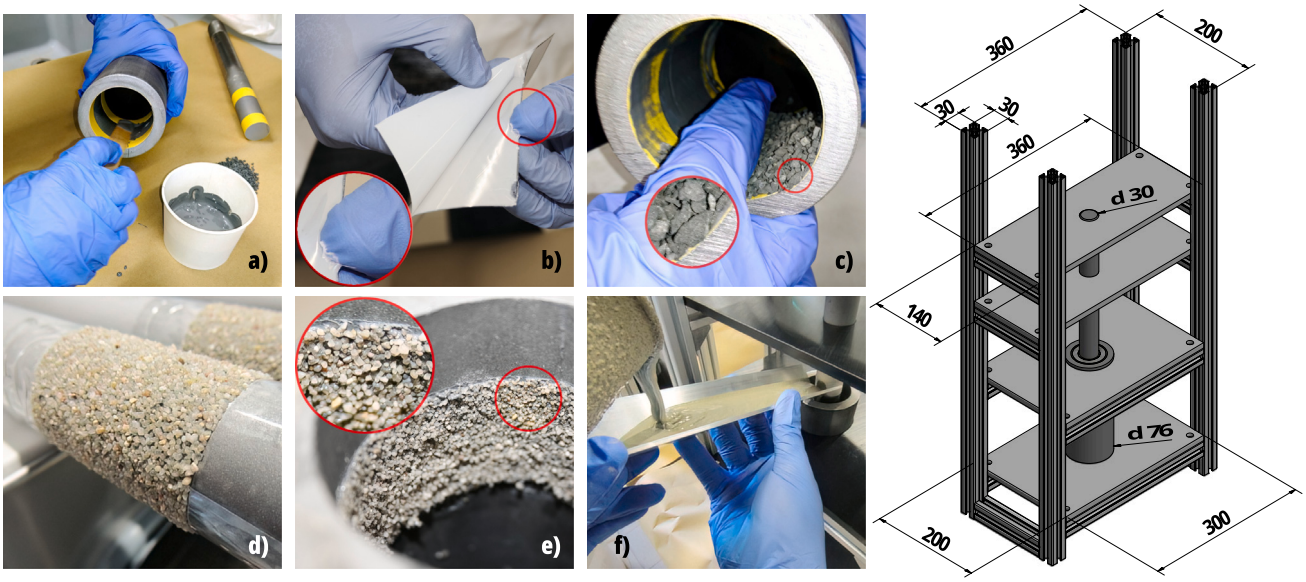

Fig. 7. Selected steps in the manufacturing of the samples — (a) Placing the liquid Sikadur370 adhesive, (b) application of the DuploTEC tape, (c) pressing the granules into the adhesive layer, (d) granules bonded onto to inner tube (pile), (e) granules bonded onto the inner side of the outer tube (sleeve), (f) grouting the gap, and (right) the pedestal used to centre the piles during the grout's 28 day curing.

Table 1
Mechanical properties of the adhesives.

Adhesive	DMA	Adhesive bulk			Lap shear	TAST		
	T_G in °C	σ_{max} in MPa	ϵ_{max} in %	E in MPa	τ_{max} in MPa	τ_{max} in MPa	γ_{max}	G in MPa
Sikadur370	75.74	21.5 ± 2.9	1.1 ± 0.4	3581 ± 113	27.50 ± 1.16	27.26 ± 6.04	0.1–0.2	882 ± 477
DuploTEC	139.50	28.7 ± 2.9	4.1 ± 2.8	1593 ± 44	27.39 ± 1.12	45.91 ± 6.29	1–3	210 ± 54

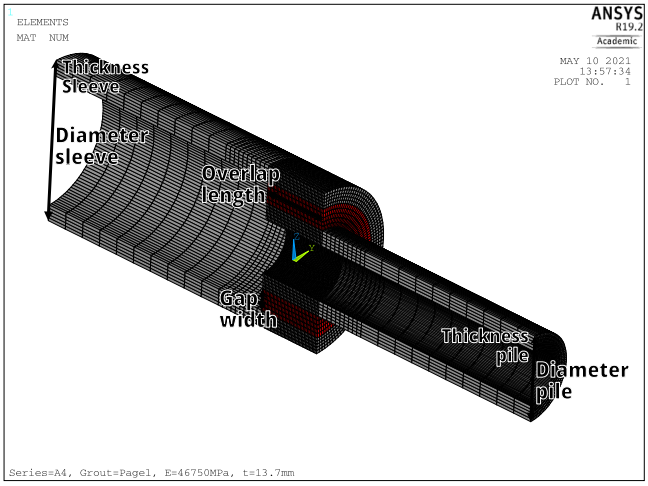

Fig. 8. Finite element model, the grout layer is represented in red.

Tests were conducted using servo-hydraulic testing machines, the tensile specimens were clamped onto fork sockets with 90° offset bolts for full rotation. Displacement control was employed with varying loading rates to achieve similar shear rates across different gap sizes. Linear Variable Differential Transformers (LVDT) were utilized to monitor relative displacement between the CHS, load, and machine displacement, with two LVDTs tracking circumferential displacement differences. Each test series consisted of 5 samples.

The tests covered a variety of parameters, including variation of the two adhesives, two overlaps, two grout gap widths, and imperfections in form of misalignment and offset of the sleeve relatively to the pile; more details being provided in the subsequent sections, and in Fig. 16. Two tube configurations were experimentally investigated. In both cases did the outer tube (or sleeve) consist of a tube with a diameter of 101.6 mm and a thickness of 10.0 mm. Two different inner tubes were tests: firstly a diameter of 48.3 mm and a thickness of 12.5 mm, leading to a gap width of 16.7 mm; secondly, a diameter of 60.3 mm and a thickness of 7.1 mm, leading to a smaller gap with of 10.7 mm.

2.4. Finite element analysis

The finite element software Ansys v19.2 was utilized for numerical modelling. The modelled joints had the same geometry as those that were experimentally investigated and were created as volume models using a symmetry plane. The Solid186 20-node element was used, mesh refinements were considered at the ends of the overlaps, where stress concentrations were expected. Along with "perfect" geometry (Fig. 8), intentional misalignment and eccentricity were also considered (Fig. 9). Only two isotropic materials were used in the model: steel (E = 210 GPa, ν = 0.3) for the tubes, and grout (Pagel'S HF 10, E = 46.75 GPa, ν = 0.2). The adhesives were not modelled separately, but their mechanical properties included in the previously presented characterization of the interface's strength (Section 2.2), and the corresponding post-processing routine described subsequently (Section 2.5).

2.5. Load capacity prediction

The implementation of the PM-based strength prediction methodology repeatedly presented in recent publications [12,16,38] so that a short recapitulation shall suffice at this point. It involves three steps: determining the stresses in the bonded joints, deriving the relevant failure criterion, and combining the previous steps to determine the load level at which the probability of survival reaches 50%.

The determination of stresses is performed according to the previously described FEA; it must deliver the relevant stresses for all grout elements and their volumes. The determination of grout's strength is based on the off-axis tests previously described in Section 2.2; it accounts for transverse normal and shear. A mathematical relationship between the stresses, the failure criterion Φ, will be derived, and its goodness of fit verified by appropriate methods, herein the Kolmogorov–Smirnov [42] and Anderson–Darling [43] Goodness-of-Fit tests.

Probabilistic methods then associates the stress level in each element to the corresponding probability of survival, whereas the term stress is broadened to consider the combined action of multiple components in the form of $\phi = \Phi(\sigma, \tau)$. For the latter, the Weibull distribution [36,37] is used to statistically describe grout's strength; this results in determining the Weibull modulus or shape parameter α, scale parameter β, and location parameter γ for Eq. (2).

$$\mathcal{P}_{S,i} = \exp\left[-\left(\frac{\phi_i - \gamma}{\beta}\right)^{\alpha}\right] \tag{2}$$

The weakest-link theory dictates that the survival probability of the entire joint is equal to the product of the survival probabilities of its individual links. This results in Equation Eq. (3), which was first derived by Freudenthal in 1968 [44] and has since then been successfully used for strength prediction [45–47].

$$\begin{aligned}\mathcal{P}_S &= \prod_{i=1}^{n} \exp\left[-\frac{V_i}{V_0}\cdot\left(\frac{\phi_i - \gamma}{\beta}\right)^{\alpha}\right] \\ &= \exp\sum_{i=1}^{n}\left[-\frac{V_i}{V_0}\cdot\left(\frac{\phi_i - \gamma}{\beta}\right)^{\alpha}\right]\end{aligned} \tag{3}$$

The replacement of the product operator (Π) with the sum (Σ) in Eq. (3) is due to the mathematical properties of the exponential function, V_i is the volume of the finite element considered and V_0 is that of the samples on which strength has been determined. The probability of survival of the joint, $\mathcal{P}_S$, depends on the load level to which the stresses are related, which is the unknown to be determined in the PM.

3. Results

3.1. Experimental results for the hybrid joints

The hybrid grout connection performed well under axial loading, demonstrating high performance and reliability. Results in terms of load-bearing capacity are given in Figs. 10a and 16. The maximum nominal shear stress on the inner tube reached 30.1 MPa, with a coefficient of variation for the load capacity averaging 5.5% across all tests. The average shear strength, Fig. 10b, was in the range of the corresponding lap shear strength reported in Table 1, although it exceeded in some cases.

The influence of the adhesive material on the hybrid grout connection was observed through load–displacement curves, with results for

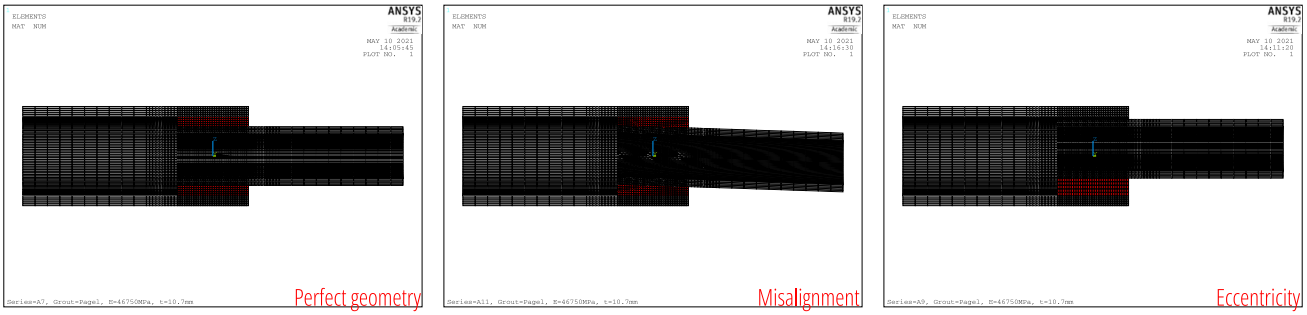

Fig. 9. Illustration of the FEA model (left) "perfect" geometry, (centre) tube's misalignment, and (right) eccentricity by offsetting the centrelines.

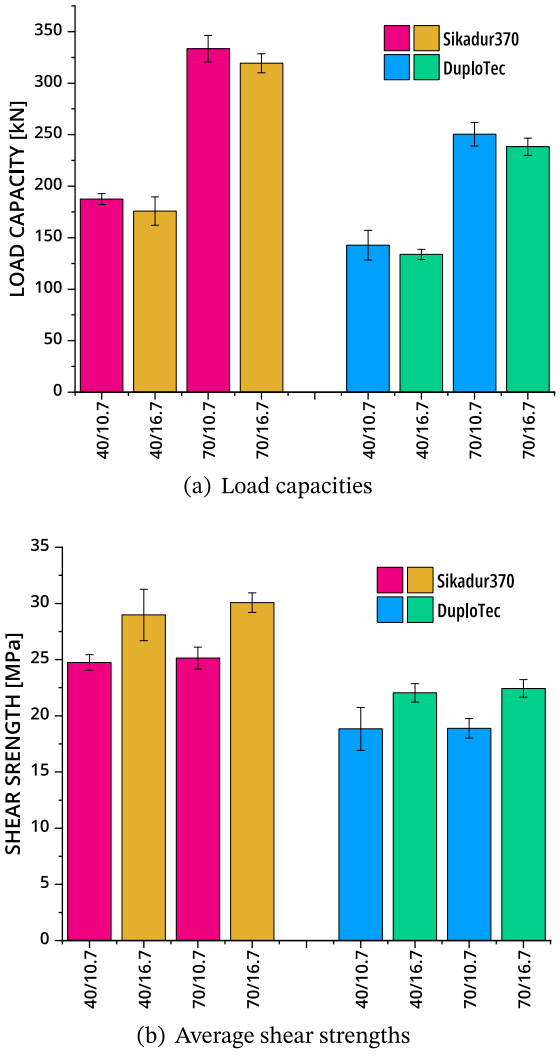

(a) Load capacities

(b) Average shear strengths

Fig. 10. Experimental results of the "perfect" hybrid joints (for those with imperfections see Fig. 16).

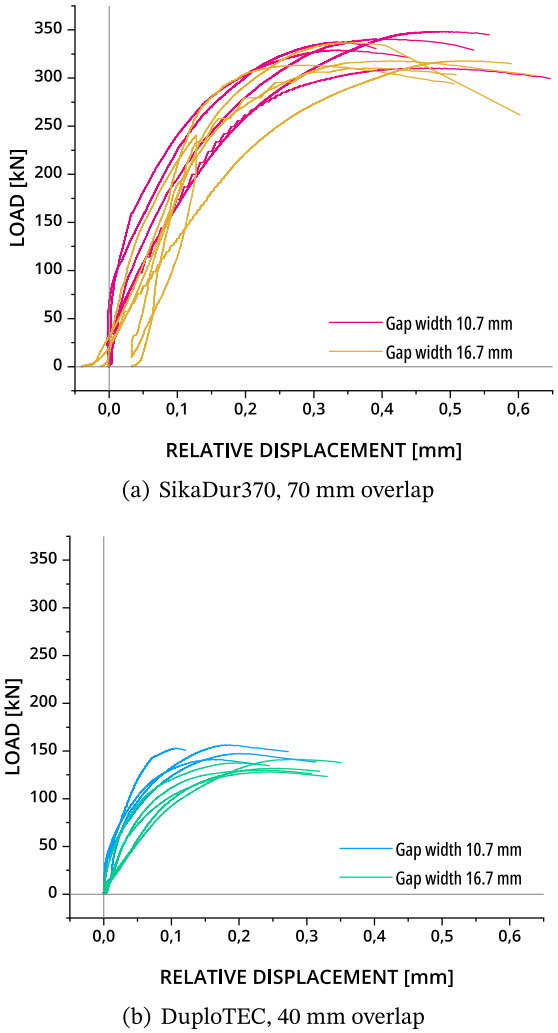

(a) SikaDur370, 70 mm overlap

(b) DuploTEC, 40 mm overlap

Fig. 11. Selected load–displacement curves of the tensile tests without imperfections.

selected series reported in Fig. 10. The stiffness of the connection was minimally affected by the adhesive's stiffness. Despite Sikadur370 having a higher elastic modulus than DuploTEC, their deformation curves in the elastic range were similar, as shows Fig. 11. The different maximum loads were not attributed to differences in lap shear strengths, listed in Table 1; in fact, based of the shear strength in the TAST-tests, opposite trends were observed. Two reasons explained the difference: the thickness of the adhesive layer and the lower elastic modulus of DuploTEC. Connections with larger gap dimensions exhibited slightly lower overall stiffness and increased relative deformation at maximum load.

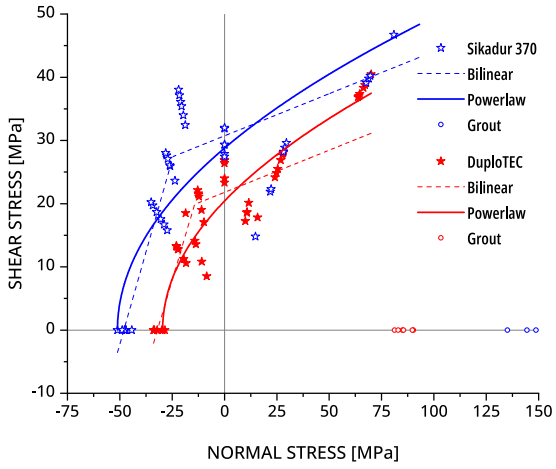

Fig. 12. Plot of the failure criteria overlaid to the corresponding experimental off-axis data.

3.1.1. Off-axis tests, failure criteria and derivation of the Weibull parameters

To formulate a failure criterion for the hybrid grout connection, a series of steps were carried out. Firstly, the failure loads obtained from off-axis tests were converted into normal and shear stresses, denoted as σ_x and τ_{xy}, respectively, using Eq. (4).

$$\begin{aligned} \sigma_x &= \sigma_0 \sin^2 \alpha \\ \tau_{xy} &= \sigma_0 \sin \alpha \cos \alpha \\ \text{with } \sigma_0 &= \frac{F_{max}}{h \times b} \end{aligned} \tag{4}$$

The resulting stress components were then plotted on a Cartesian coordinate system, as illustrated in Fig. 12, which indicates that shear strength is significantly lower for tensile normal stresses as compared to compressive normal stresses. Moreover, it was observed that the adhesive Sikadur370 consistently achieved higher strengths than the DuploTEC adhesive tape. The trend for shear strength as a function of normal stresses appears to be asymptotic, rather than linear as would be expected from a simple linear friction model. The minimum tensile normal stress for SikaDur370 was found to be around −50 MPa, while it was approximately −30 MPa for DuploTEC; both are higher than the corresponding tensile strength reported in Table 1. The data from off-axis tests were analysed with the OriginPro2019 statistical software package using two fitting functions: Φ_1, Eq. (5), a power-law expression, and Φ_2, Eq. (6), a bilinear approximation.

$$\tau = a \times (\sigma - \sigma_c)^c \tag{5}$$

$$\tau = \begin{cases} a_1 + k_1 \times \sigma, & \text{if } \sigma < \sigma_i \\ a_2 + k_2 \times (\sigma - \sigma_i), & \text{otherwise} \end{cases} \tag{6}$$

Table 2 summarizes the mathematical expressions, corresponding parameters, and Goodness of Fit (GoF) metrics for both models. The GoF analysis was supported by a visual comparison in Fig. 12. Since the power-law fit performed slightly better than the bilinear fit in terms of GoF, the investigation with the latter was stopped. For the power-law model, the exponent values of $c = 0.53 \pm 0.04$ for Sikadur370 and $c = 0.48 \pm 0.04$ for DuploTEC were both approximated to $c = 0.5$, resulting in a slightly easier to implement quadratic interaction formula for the power-law.

A failure criterion serves as the boundary between survival ($\phi_i \leq 1$) and failure ($\phi_i > 1$). Next, it is essential to find the scaling factor λ_i that would make a stress combination reach failure ($\phi_i = 1$), which is the distance between the considered stress state and the failure envelope. As shown in [16], for the power-law fit-function λ_i can be determined

Table 2
Parameters for the fitting curves.

	Power-law, Φ_1	Bilinear, Φ_2
Sikadur370	$a = 3.75 \pm 0.15$ $\sigma_u = -29.6 \pm 1.83$ $c = 0.53 \pm 0.04$ c is set to 0.5	$a_1 = 35.90 \pm 6.91$ $k_1 = 1.12 \pm 0.26$ $\sigma_I = -15.11 \pm 3.32$ $k_2 = 0.13 \pm 0.06$
	Red. $\chi^2 = 20.3$ R^2 (COD) = 0.788 Adj. $R^2 = 0.783$	Red. $\chi^2 = 27.4$ R^2 (COD) = 0.799 Adj. $R^2 = 0.788$
DuploTEC	$a = 4.03 \pm 0.18$ $\sigma_u = -51.11 \pm 3.34$ $c = 0.48 \pm 0.04$ c is set to 0.5	$a_1 = 56.16 \pm 1.52$ $k_1 = 1.16 \pm 0.03$ $\sigma_I = -24.58 \pm 2.36$ $k_2 = 0.133 \pm 0.03$
	Red. $\chi^2 = 66.78$ R^2 (COD) = 0.66 Adj. $R^2 = 0.65$	Red. $\chi^2 = 39.32$ R^2 (COD) = 0.80 Adj. $R^2 = 0.79$

by solving Eq. (7), with σ_i and τ_i the stress state under consideration, and a and σ_c defined by Table 2.

$$\lambda_i = \frac{a^2\sigma_i \pm \sqrt{a^4\sigma_i^2 - 4a^2\sigma_c\tau_i^2}}{2\tau_i^2} \tag{7}$$

For illustration, Fig. 13 graphically represents the λ_i-values determined for both Sikadur370 and DuploTEC; it shows that all experimental results below the failure envelope result in $\lambda_i < 1$, while for those above Eq. (7) results in $\lambda_i > 1$; the line for which $\lambda = 1$ being the corresponding failure criterion.

Afterwards, the statistical characteristics of the λ-values distribution for Sikadur370 and DuploTEC were determined by assuming a three-parameter Weibull distribution—defined by Eq. (2). The Weibull parameters were determined using the EasyFit software and resulted in the following outcomes: $\alpha = 4.468$, $\beta = 0.889$, $\gamma = 0.242$ for Sikadur370, and $\alpha = 1.348$, $\beta = 0.431$, $\gamma = 0.638$ for DuploTEC. Kolmogorov–Smirnov [42] and Anderson–Darling [43] Goodness-of-Fit tests were carried out with a significance level of 0.05, and neither did reject the hypothesis that the data was Weibull-distributed.

3.2. Computational strength prediction

3.2.1. Stresses in the hybrid joints

The stresses considered in this study were primarily normal stresses acting in radial directions (or through thickness stresses, denoted by the subscript R for radial) and shear stresses in the XR plane (where X is axial). These stress components were determined for all subsequent test series using a reference load of $F_0 = 200$ kN. This reference load was chosen to allow a comprehensive evaluation of the effects of each varied parameter.

At both ends of the overlap, noticeable peaks were observed in the through-thickness (or normal) stresses (σ_R) and shear stresses (τ_{XR}), as shown in Fig. 14. In particular, these stress components showed higher peak values below the 'ends' of the tubes. The results also showed that for a comparable axial load (0 = 200 kN), the stress peaks were dependent on the overlap length, with peak values of both σ_R and τ_{XR} increasing as the overlap length decreased, as shown in Fig. 14a and b. Fig. 14c and d show the influence of the width of the joint; the peaks of σ_R and τ_{XR} were only marginally affected and the influence was only evident in the evolution along the overlap.

When geometric imperfections such as misalignment and eccentricity were included, both the through thickness normal stresses (R) and shear stresses (XR) changed compared to the reference case, as shown in Fig. 14e to h. The Finite Element Analysis (FEA) results showed that the offset of the pipe centrelines had a moderate effect on both the through thickness (or normal) stresses σ_R and shear stresses τ_{XR} within

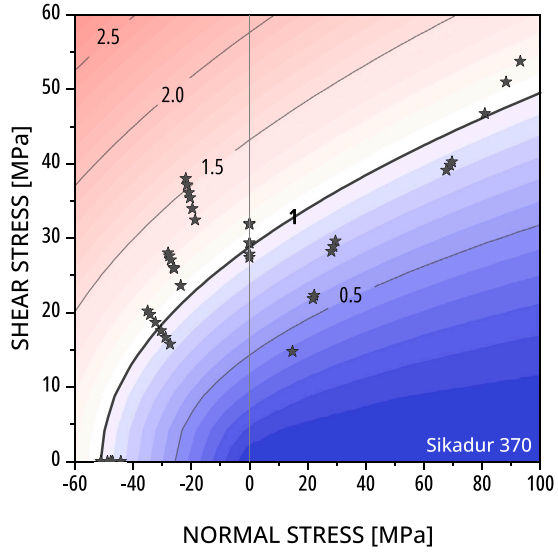

(a) Sikadur370

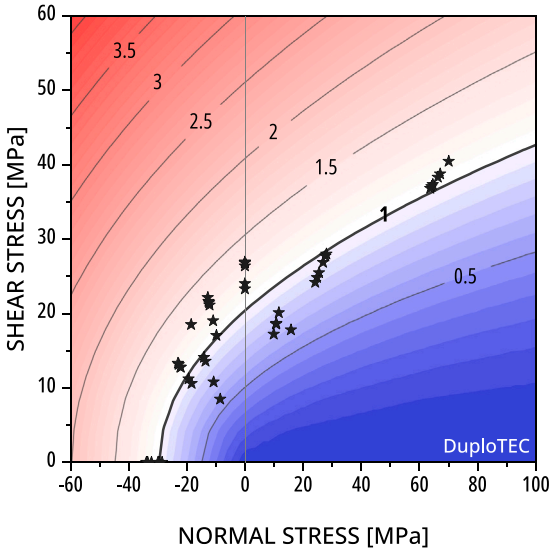

(b) DuploTEC

Fig. 13. Graphical representation of the λ-values, where measurements above the failure criterion (in variable shades of red) exceed the mean strength value and exhibit $\lambda > 1$, while measurements below the criterion (in blue) indicate less mechanical utilization and exhibit $\lambda < 1$. The failure criterion, $\lambda = 1$, is the thick black line.

the overlap region. The most significant effect was observed at the beginning of the overlap, where both peak stress values nearly doubled. However, along most of the overlap length no significant effects were observed.

At the end of the overlap (position 0 mm) the peak shear stress increased moderately, while no such effect was observed for the through-thickness stresses. Intentionally misaligning the centre lines of the tubes also resulted in increased peak stress values at both ends. However, compared to offsetting, misalignment at the end of the overlap had a more pronounced effect, particularly for the through-thickness stresses (approximately a 50% increase in magnitude). In addition, the shear stresses showed slight changes over the entire overlap length.

Looking at the radial distribution at the end of the overlap (the most stressed position), the influence of the misalignment is evident from Fig. 15. In the reference situation, both normal stresses (σ_R) and shear stresses (τ_{XR}) remained constant. However, tilting the axis caused a noticeable shift in both stress components. The magnitudes of these stresses were significantly reduced in regions where the adhesive layer was thicker (Fig. 15), while they increased by approximately 50% at the opposite end (also Fig. 15).

For the strength prediction of the hybrid joints, it is proposed, in accordance with the experimental observation and the FEA, that the failure of the hybrid joints is mainly influenced by two stress components: σ and τ. Their mutual effect on the strength was evaluated in the off-axis tests by the failure criterion Φ. For each element of the model section, the failure criterion value $\phi_i = \Phi(\sigma_i, \tau_i)$ was calculated and assigned a failure probability using the relationships developed earlier in Section 2.5. For the purposes of the following discussion, it is assumed that the initiation of failure is confined to the adhesive/steel interface and that the probability of each element is equal to that of the off-axis specimens.

The first step was to estimate the load capacity of the experimentally tested joints. Fig. 16 shows the load capacities obtained from experiments and predictions, together with the corresponding overlap lengths and joint gap dimensions. On average, the predicted load capacities were found to be underestimated by approximately 5% and did not show significant dependence on the type of adhesive used. However, it is important to recognize the statistical variability of the experimental data, with an average standard deviation ranging from an underestimation of 16% to an overestimation of 7%. Overall, the authors assert that the prediction method has provided reliable estimates of load-bearing capacity.

Based on the validation, the influence of geometric dimension and the effects of eccentricity and misalignment on load capacity were modelled. The results are summarized in Fig. 16.

The results partially confirm the expected results. For example, it was expected that the load carrying capacity of the hybrid grouted joints would increase with overlap length, but this increase was found to be non-linear and converged to an upper value. Within the range investigated, the thickness of the joint gap appeared to have little effect, which, while confirming the experimental evidence, is surprising. The effect of misalignment was not as significant as expected, and substantial misalignment is required to observe a significant reduction in strength; the same was observed for eccentricity. Judging by the quantitative agreement between the predicted and experimentally determined load capacities, Fig. 16 shows that the methodology was accurate.

3.3. Additional modelling and prediction

In a last step, a much larger, but otherwise similar, hybrid grouted joint, fully described in [40], was numerically simulated to predict its load-bearing capacity. For this large-scale set of specimens, the dimensions of the sleeve (outer tube) were $D/t = 273/20$ (both in mm), and that of the pile (inner tube) $D/t = 193.7/20$ (both in mm), which resulted in a nominal gap of 19.7 mm. The overlap length was set to 150 mm. For this series, the only material combination investigated was Sikadur-370, Pagel HF10, and quartz sand. The load was applied in compression, and not in tension.

Globally, the load-bearing behaviour until failure was analogous to the experiments described previous. The load increased almost linearly until reaching the maximum load. The maximum load was reached at an average of 1673 ± 108 kN, the corresponding average shear strength on the inner tube (pile) amounted to 18.3 MPa. It was notable that two specimens reached a load of more than 1700 kN (1717 kN and 1752 kN, or 1734 ± 25 kN if restricting the series thereon), while the third specimen failed at 1550 kN.

Based upon the very same load capacity prediction procedure described previous, and considering that for this series the load was compression, three different scenarios were considered: element selection for Eq. (3) was restricted to the interface with the inner tube (or pile, if maintaining the offshore terminology, cf. Fig. 17-top), at the interface with the outer tube (or sleeve, cf. Fig. 17-middle), and failure at

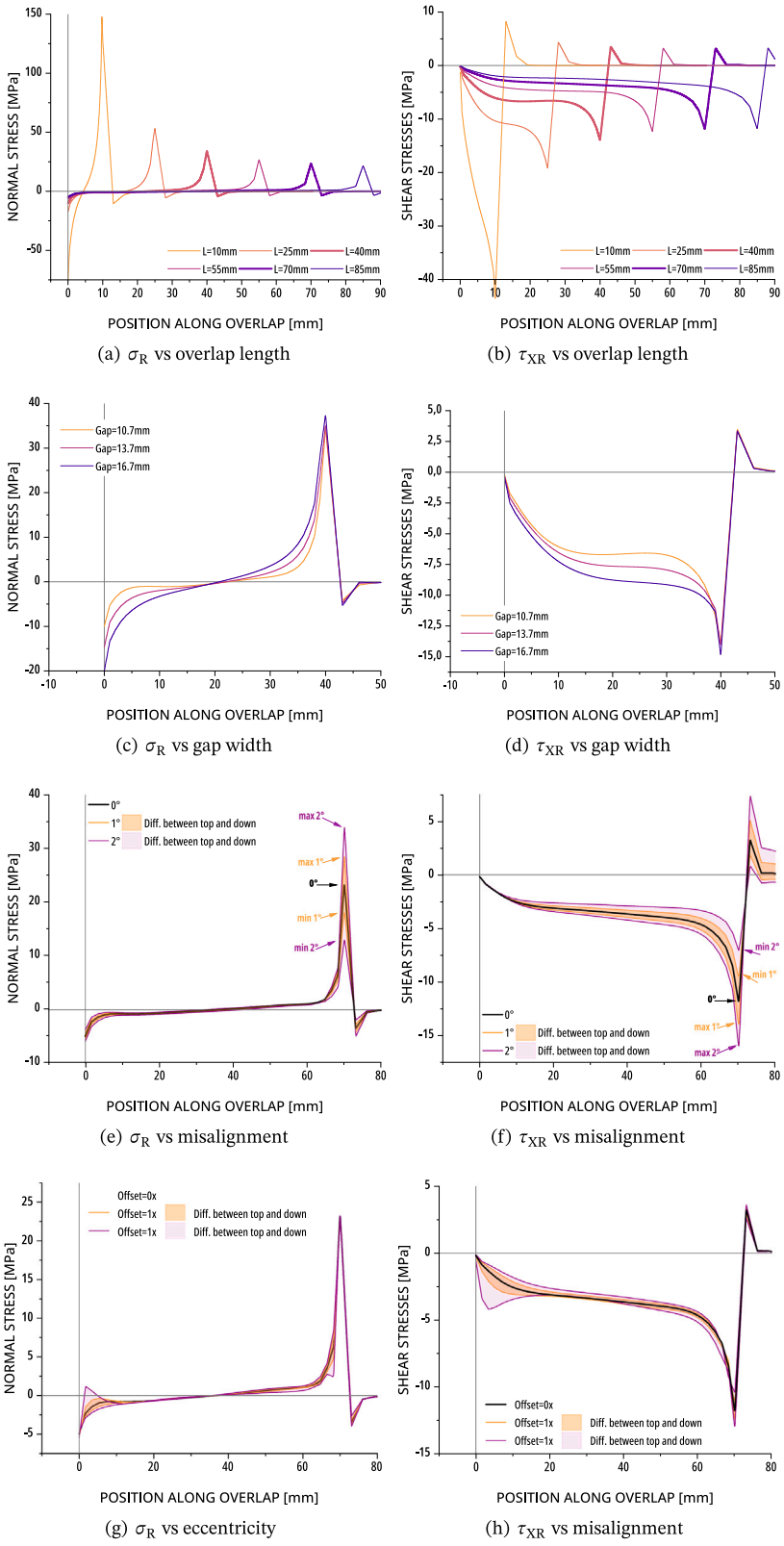

(a) σ_R vs overlap length (b) τ_{XR} vs overlap length

(c) σ_R vs gap width (d) τ_{XR} vs gap width

(e) σ_R vs misalignment (f) τ_{XR} vs misalignment

(g) σ_R vs eccentricity (h) τ_{XR} vs misalignment

Fig. 14. Influence of various parameters on normal and shear stresses along the overlap for a reference load of F_0 = 200 kN.

both the inner and outer tubes (as considered in the prior examples, or Fig. 17-bottom). Restriction of the elements in essence corresponds to make a pre-supposition of the failure location according to Fig. 17. The corresponding calculated load capacities are summarized in Table 3.

The analysis revealed that considering only the interface with the inner tube resulted in a predicted load capacity of 1926 kN. Allowing failure only at the interface with the outer tube (sleeve) increased this capacity by almost 2/3 to an unrealistic value of 3234 kN. However,

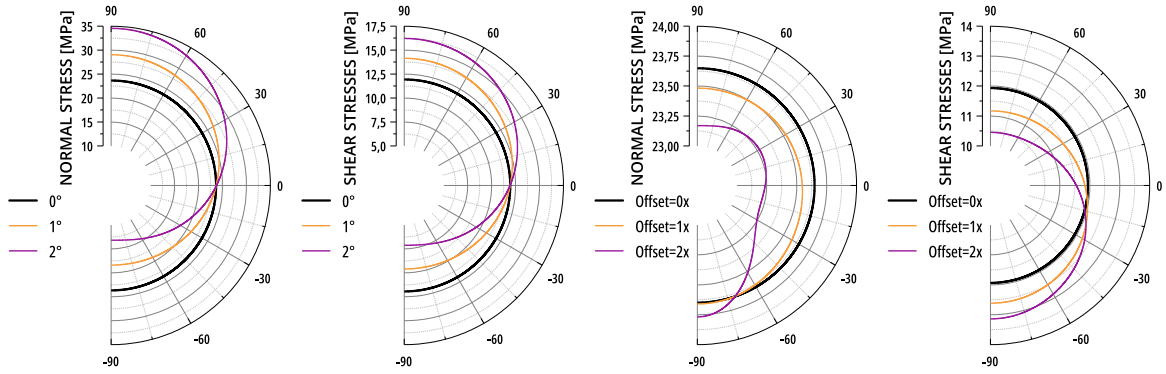

(a) σ_R vs misalignment (b) τ_{XR} vs misalignment (c) σ_R vs eccentricity (d) τ_{XR} vs eccentricity

Fig. 15. Influence of misalignment and eccentricity on the normal and shear stresses at the end of the overlap.

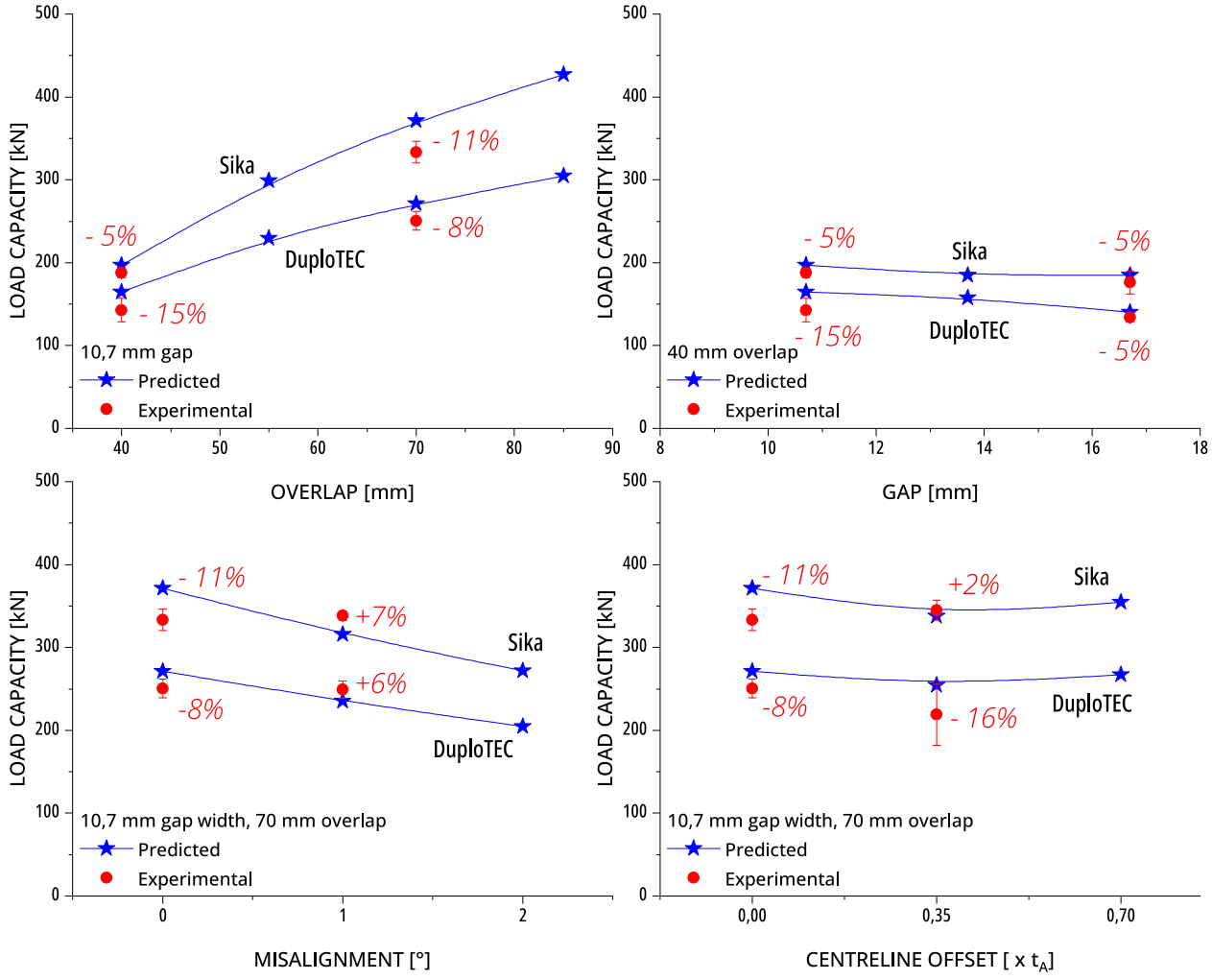

Fig. 16. Predicted vs. experimentally determined (if available) load capacities of the hybrid joints; the percentages indicate the relative deviation from predicted to experimental values.

Table 3
Load capacity of the large-scale hybrid grouted joint.

Consideration of the interface	Predicted [kN]	Experimental [kN]		Rel. deviation [%]	
		With outlier	Without outlier	With outlier	Without outlier
Only at the pile (inner tube)	1926			15%	11%
Only at the sleeve (outer tube)	3234	1673 ± 108	1734 ± 25	93%	86%
At both the sleeve and the pile	1906			14%	10%

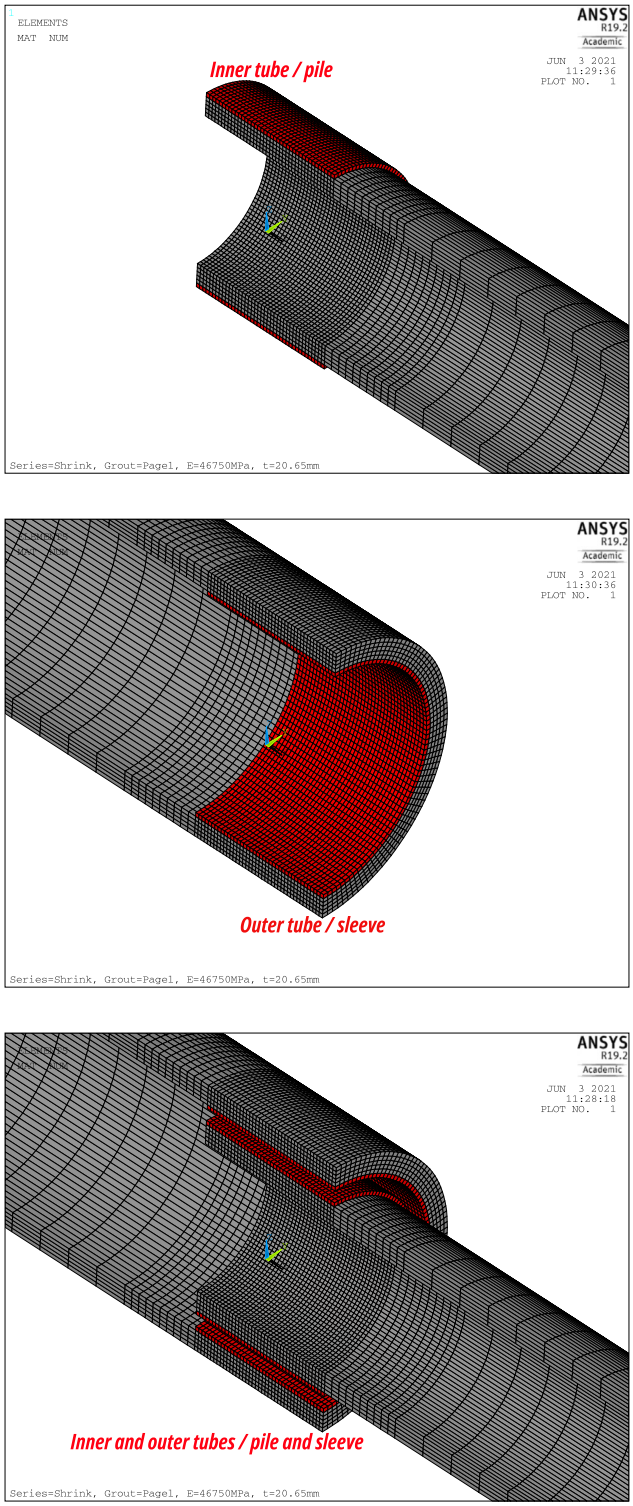

Fig. 17. FE-model of the large-scale grouted hybrid joint (top) the pile with the adhesive layer at the outside, (middle) the sleeve with the adhesive at the inside, and (bottom) adhesive layers on both the pile and the sleeve.

simultaneous consideration of the interfaces at both the inner and outer tubes led to a slight reduction in load capacity to approximately 1900 kN. Therefore, the numerical analysis suggests that the critical interface is the one with the inner tube, which the post-failure analysis confirms. When comparing these results with the experimental values, it should be noted that a significant outlier was observed in the experiments. Considering this outlier, the deviation between the numerical and experimental values is 14%; excluding it decreases to approximately 10% when excluding the outlier from the calculation of the experimental mean value.

4. Discussion and conclusions

The hybrid joint, the focus of this publication, demonstrated robust performance and reliability under axial loading. The maximum nominal shear stress on the inner tube reached 30.1 MPa and showed a consistent load capacity across the tests, with a low coefficient of variation averaging 5.5%. The average shear strength was within the expected range and occasionally exceeded it. The comparison of load capacities demonstrated the resilience of the joint in different configurations. In particular, the coefficient of variation for load capacity remained low, indicating consistent performance. The average shear strength was in line with expectations. When the influence of the adhesive material on the hybrid grout joint was examined using load–displacement curves, minimal effect on joint stiffness was observed despite variations in adhesive stiffness. Sikadur370, which has a higher modulus of elasticity than DuploTEC, showed similar deformation curves in the elastic region, emphasizing the robustness of the joint. Differences in maximum loads were attributed to the thickness of the adhesive layer and the lower modulus of DuploTEC, resulting in different shear strengths. In summary, the hybrid grout joint demonstrated consistent and reliable performance, with load capacities and shear strengths meeting or exceeding expectations. The low coefficients of variation indicate stability across different configurations, demonstrating the suitability of the joint for a variety of engineering applications.

The formulation of a failure criterion for the hybrid joint involved several key steps. First, the failure loads from the off-axis tests were converted into normal (σ_x) and shear (τ_{xy}) stresses. The resulting stress components were then plotted on a Cartesian coordinate system, revealing a significant difference in shear strength between tensile and compressive normal stresses. In particular, Sikadur370 showed consistently higher strengths compared to DuploTEC tape. The relationship between shear strength and normal stresses showed an asymptotic trend which differed from the expected linear friction model. The minimum tensile normal stress for SikaDur370 was approximately −50 MPa and for DuploTEC it was approximately −30 MPa.

The numerical study focused on the analysis of stresses in hybrid grouted joints. Throughout the investigation, noticeable peaks in both through thickness (or normal) stresses (σ_R) and shear stresses (τ_{XR}) were observed at both ends of the overlap. These stress components had higher peak values below the 'ends' of the pipes. Analysis showed that for a comparable axial load ($F_0 = 200$ kN) the stress peaks were dependent on the overlap length, decreasing with increasing peak values for both σ_R and τ_{XR}. Investigation of the influence of joint width showed that the peaks of σ_R and τ_{XR} were only marginally affected, with the influence evident in the evolution along the overlap.

Incorporating misalignment and eccentricity altered both the through-thickness normal stresses (σ_R) and shear stresses (τ_{XR}). Finite Element Analysis (FEA) showed that the offset pipe centrelines moderately affected both σ_R and τ_{XR} within the overlap region, with the most significant effect at the beginning of the overlap where peak stress values almost doubled. Towards the end of the overlap (position 0 mm), the peak shear stress increased moderately, whereas there was no significant effect on the through-thickness stresses. Intentional misalignment of the tube centrelines increased the peak stress values at both ends. However, misalignment at the end of the overlap had a more pronounced effect, particularly on the through-thickness stresses, resulting in an increase in magnitude of approximately 50%. Shear stresses showed little change over the entire overlap length. The radial distribution at the end of the overlap highlighted the influence of misalignment, causing a noticeable shift in both stress components. Stress magnitudes decreased in regions with a thicker adhesive layer and increased by approximately 50% at the opposite end.

For the strength prediction of hybrid joints, the study proposed, in agreement with experimental observations and FEA, that the failure of hybrid joints is mainly influenced by two stress components: σ and τ. Their mutual effect on strength was evaluated in off-axis tests using a failure criterion. Failure initiation was assumed to be confined to the adhesive/steel interface. Estimation of the load-bearing capacity of the experimentally tested joints showed an average underestimation of about 5%, with a standard deviation ranging from an underestimation of 16% to an overestimation of 7%. The authors concluded that the prediction method provided reliable estimates of load capacity.

Based on the validation, the influence of geometric dimensions and the effects of eccentricity and misalignment on load capacity were modelled. The results partially confirmed expectations, such as the non-linear increase in load capacity with overlap length, converging to an upper value. Contrary to initial expectations, gap thickness had little effect over the range studied. The effects of misalignment and eccentricity were not as significant as expected, with significant misalignment required to observe a significant reduction in strength. A final step was to numerically simulate a larger scale hybrid grouted joint. The numerical analysis suggested that the critical interface for failure was with the inner tube, in agreement with the post-failure analysis. Considering different failure scenarios, the predictions showed significant percentage deviations from the experimental values. The critical interface was identified as the one with the inner tube, with a percentage deviation of approximately 14%, reduced to 10% when excluding a significant outlier.

In summary, the study provides a thorough investigation of the stress distribution and the effects of various parameters on the load carrying capacity of hybrid joints. It also highlights the sensitivity of joint behaviour to factors such as overlap length, tube diameter and geometric imperfections. The methodology's accuracy in predicting load capacity, supported by numerical analysis and large-scale joint simulations, contributes to a comprehensive understanding, and trust, of hybrid joint performance in engineering applications. While the initial impetus for this study came from the offshore industry, it has a much wider applications field, for example when considering bridge structures composed of tubular sections. This is not to say that there are questions remaining unanswered. Future studies should focus on aspects as long-term durability under severe environmental conditions and fatigue. Due to the presence of the adhesive, aspects as temperature (in particular above glass transition temperature) and creep do certainly require more extensive attention.

CRediT authorship contribution statement

Sebastian Myslicki: Conceptualization, Data curation, Formal analysis, Funding acquisition, Project administration, Software, Supervision, Validation, Visualization, Writing – original draft, Writing – review & editing. **Till Vallée:** Supervision, Visualization, Writing – review & editing. **Marvin Kaufmann:** Validation, Writing – review & editing. **Thomas Ummenhofer:** Supervision, Writing – review & editing. **Jakob Boretzki:** Data curation, Investigation, Project administration, Visualization. **Matthias Albiez:** Data curation, Investigation, Validation, Writing – review & editing.

Declaration of competing interest

The authors declare the following financial interests/personal relationships which may be considered as potential competing interests: Sebastian Myslicki reports financial support was provided by Allianz Industrieforschung. Sebastian Myslicki reports a relationship with Federal Ministry for Economy and Energy that includes: funding grants.

Data availability

Data will be made available on request.

Acknowledgements

This research was supported by the German Federal Ministry of Economic Affairs and Climate Action through the German Federation of Industrial Research Associations (AiF) as part of the program for promoting industrial cooperative research (project IGF 19989 N of the Research Association for Steel Application – FOSTA).

Additionally, the authors want to express their sincere gratitude for the help of Louisa Lucas for proofreading.

References

[1] Klose M, Faber T, Schaumann P, Lochte-Holtgreven S. Grouted connections for offshore wind turbines. In: International ocean and polar engineering conference. Vol. All Days, 2008, URL https://onepetro.org/ISOPEIOPEC/proceedings-abstract/ISOPE08/All-ISOPE08/ISOPE-I-08-033/10798. ISOPE-I-08-033.

[2] Schaumann P, Wilke F. Design of large diameter hybrid connections grouted with high performance concrete. In: International ocean and polar engineering conference. Vol. All Days, 2007, URL https://onepetro.org/ISOPEIOPEC/proceedings-abstract/ISOPE07/All-ISOPE07/ISOPE-I-07-266/11864. ISOPE-I-07-266.

[3] Tziavos NI, Hemida H, Metje N, Baniotopoulos C. Grouted connections on offshore wind turbines: a review. Proc Inst Civ Eng-Eng Comput Mech 2016;169(4):183–95. http://dx.doi.org/10.1680/jencm.16.00004.

[4] Schmidt M, Fehling E, Braun T. Grouted connections for offshore wind turbine structures. Steel Constr 2013;6(3):207–15. http://dx.doi.org/10.1002/stco.201310032.

[5] Fehling E, Leutbecher T, Schmidt M, Ismail M. Grouted connections for offshore wind turbine structures. Steel Constr 2013;6(3):216–28. http://dx.doi.org/10.1002/stco.201310031.

[6] Billington CJ, Lewis GH. The strength of large diameter grouted connections. In: OTC offshore technology conference. Vol. All Days, 1978, http://dx.doi.org/10.4043/3083-MS, OTC-3083-MS.

[7] Billington CJ, Tebbett IE. The basis for new design formulae for grouted jacket to pile connections. OTC offshore technology conference, vol. All Days, 1980, http://dx.doi.org/10.4043/3788-MS.

[8] Solland G, Johansen A. Design recommendations for grouted pile sleeve connections. Mar Struct 2018;60:1–14. http://dx.doi.org/10.1016/j.marstruc.2018.03.001.

[9] Lamport WB, Jirsa JO, Yura JA. Strength and behavior of grouted pile-to-sleeve connections. J Struct Eng 1991;117(8):2477–98. http://dx.doi.org/10.1061/(ASCE)0733-9445(1991)117:8(2477).

[10] Krahl NW, Karsan DI. Axial strength of grouted pile-to-sleeve connections. J Struct Eng 1985;111(4):889–905. http://dx.doi.org/10.1061/(ASCE)0733-9445(1985)111:4(889).

[11] Albiez M, Vallée T, Fricke H, Ummenhofer T. Adhesively bonded steel tubes — Part I: Experimental investigations. Int J Adhes Adhes 2019;90:199–210. http://dx.doi.org/10.1016/j.ijadhadh.2018.02.005.

[12] Albiez M, Vallée T, Ummenhofer T. Adhesively bonded steel tubes – part II: Numerical modelling and strength prediction. Int J Adhes Adhes 2019;90:211–24. http://dx.doi.org/10.1016/j.ijadhadh.2018.02.004.

[13] Albiez M, Damm J, Ummenhofer T, Kaufmann M, Vallée T, Myslicki S. Hybrid joining of jacket structures for offshore wind turbines € determination of requirements and adhesive characterisation. Eng Struct 2022;259:114186. http://dx.doi.org/10.1016/j.engstruct.2022.114186.

[14] Albiez M, Damm J, Ummenhofer T, Ehard H, Schuler C, Kaufmann M, Vallée T, Myslicki S. Hybrid joining of jacket structures for offshore wind turbines — validation under static and dynamic loading at medium and large scale. Eng Struct 2022;252:113595. http://dx.doi.org/10.1016/j.engstruct.2021.113595.

[15] Denkert C, Gerke T, Glienke R, Dörre M, Henkel MK, Fricke H, Myslicki S, Kaufmann M, Vallée MVT. Experimental investigations on pre-tensioned hybrid joints for structural steel applications. J Adhes 2023;99(2):117–52. http://dx.doi.org/10.1080/00218464.2021.2003786.

[16] Vallée T, Fricke H, Myslicki S, Kaufmann M, Denkert MVC, Glienke R, Dörre M, Henkel M-K, Gerke T. Modelling and strength prediction of pre-tensioned hybrid bonded joints for structural steel applications. J Adhes 2022;98(11):1573–613. http://dx.doi.org/10.1080/00218464.2021.1928498.

[17] Dallyn P, El-Hamalawi A, Palmeri A, Knight R. Experimental testing of grouted connections for offshore substructures: A critical review. Structures 2015;3:90–108. http://dx.doi.org/10.1016/j.istruc.2015.03.005.

[18] Schaumann P, Lochte-Holtgreven S, Eichstädt R, Camp T, McCann G. Numerical investigations on local degradation and vertical misalignments of grouted joints in monopile foundations. In: International ocean and polar engineering conference. Vol. All Days, 2013, URL https://onepetro.org/ISOPEIOPEC/proceedings-abstract/ISOPE13/All-ISOPE13/ISOPE-I-13-173/15262. ISOPE-I-13-173.

[19] Yokozeki K, Evers T, Vallée T. Impact of joint geometries in bonded-bolted hybrid joints for steel construction. Journal of Constructional Steel Research 2023;211:108166. http://dx.doi.org/10.1016/j.jcsr.2023.108166.

[20] Yokozeki K, Hisazumi K, Vallée T, Evers T, Ummenhofer T, Boretzki J, Albiez M. Hybrid joints consisting of pre-tensioned bolts and a bonded connection, part II: Large-scale experiments. Int J Adhes Adhes 2024;128:103523. http://dx.doi.org/10.1016/j.ijadhadh.2023.103523.

[21] Desch C. General discussion on cohesion and related problems. Cohesion: a general survey. Trans Faraday Soc 1928;24:53–64.

[22] Wake W. Theories of adhesion and uses of adhesives: a review. Polymer 1978;19(3):291–308. http://dx.doi.org/10.1016/0032-3861(78)90223-9.

[23] Kozma L, Olefjord I. Surface treatment of steel for structural adhesive bonding. Mater Sci Technol 1987;3(11):954–62. http://dx.doi.org/10.1179/mst.1987.3.11.954.

[24] Da Silva LF, Öchsner A, Adams RD. Introduction to adhesive bonding technology. In: Handbook of adhesion technology. Springer; 2018, p. 1–7.

[25] Adams RD, editor. Adhesive bonding: Science, technology and applications. Woodhead publishing series in materials, 2nd ed.. Oxford: Woodhead Publishing; 2021.

[26] De Bruyne N-A. The strength of glued joints. Aircr Eng Aerosp Technol 1944. http://dx.doi.org/10.1108/eb031117.

[27] Volkersen O. Die nietkraftverteilung in zugbeanspruchten nietverbindungen mit konstanten laschenquerschnitten. Luftfahrtforschung 1938;15(1/2):41–7.

[28] Adams R, Peppiatt N. Stress analysis of adhesive-bonded lap joints. J Strain Anal 1974;9(3):185–96. http://dx.doi.org/10.1243/03093247V093185.

[29] Broberg K. Critical review of some theories in fracture mechanics. Int J Fract Mech 1968;4:11–9. http://dx.doi.org/10.1007/BF00189139.

[30] Elices M, Guinea G, Gómez J, Planas J. The cohesive zone model: advantages, limitations and challenges. Eng Fract Mech 2002;69(2):137–63. http://dx.doi.org/10.1016/S0013-7944(01)00083-2.

[31] Chaves FJP, da Silva LFM, de Moura MFSF, Dillard DA, Esteves VHC. Fracture mechanics tests in adhesively bonded joints: A literature review. J Adhes 2014;90(12):955–92. http://dx.doi.org/10.1080/00218464.2013.859075.

[32] Zhang J, Wang J, Yuan Z, Jia H. Effect of the cohesive law shape on the modelling of adhesive joints bonded with brittle and ductile adhesives. Int J Adhes Adhes 2018;85:37–43. http://dx.doi.org/10.1016/j.ijadhadh.2018.05.017.

[33] Till Vallée, Marvin Kaufmann, Robert D Adams, Matthias Albiez, João R Correia, Thomas Tannert. Are probabilistic methods a way to get rid of fudge factors? Part I: Background and theory. Int J Adhes Adhes 2022;119:103255. http://dx.doi.org/10.1016/j.ijadhadh.2022.103255.

[34] Santos T, Campilho R. Numerical modelling of adhesively-bonded double-lap joints by the extended finite element method. Finite Elem Anal Des 2017;133:1–9. http://dx.doi.org/10.1016/j.finel.2017.05.005.

[35] Tsai C, Guan Y, Ohanehi D, Dillard J, Dillard D, Batra R. Analysis of cohesive failure in adhesively bonded joints with the SSPH meshless method. Int J Adhes Adhes 2014;51:67–80. http://dx.doi.org/10.1016/j.ijadhadh.2014.02.009.

[36] Weibull W. A statistical theory of strength of materials. Ing Vetensk Akad Handl 1938. (Nr. 151).

[37] Weibull W. The phenomenon of rupture in solids. Ing Vetensk Akad Handl 1939. (Nr. 153).

[38] Vallée T, Kaufmann M, Adams RD, Albiez M, Correia JR, Tannert T. Are probabilistic methods a way to get rid of fudge factors? Part II: Application and examples. Int J Adhes Adhes 2023;124:103364. http://dx.doi.org/10.1016/j.ijadhadh.2023.103364.

[39] de Coulomb C-A. Essai sur une application des regles de maximis et minimis a quelques problemes de statique relatifs a l'architecture. 1773;7.

[40] Boretzki J, Albiez M, Myslicki S, Vallée T, Ummenhofer T. Hybrid grouted joints: Load bearing and failure behaviour under static, axial loading. Constr Build Mater 2023;413:103364. http://dx.doi.org/10.1016/j.conbuildmat.2023.134691.

[41] Myslicki S, Vallée T, Fricke H, Ummenhofer T, Boretzki J, Albiez M. Hybrid grouted steel connections using adhesively bonded granules in the steel grout interface: Development and validation of an innovative joining technique. Constr Build Mater 2023. http://dx.doi.org/10.1016/j.conbuildmat.2023.134765.

[42] Frank J, Massey J. The Kolmogorov-Smirnov test for goodness of fit. J Amer Statist Assoc 1951;46(253):68–78. http://dx.doi.org/10.1080/01621459.1951.10500769.

[43] Anderson TW, Darling DA. Asymptotic theory of certain "goodness of fit" criteria based on stochastic processes. Ann Math Stat 1952;23(2):193–212, URL https://www.jstor.org/stable/2236446.

[44] Freudenthal AM. Statistical approach to brittle fracture. Fract Adv Treatise II 1968;591–619.

[45] Vallée T, Correia JR, Keller T. Probabilistic strength prediction for double lap joints composed of pultruded GFRP profiles – part II: Strength prediction. Compos Sci Technol 2006;66(13):1915–30. http://dx.doi.org/10.1016/j.compscitech.2006.04.001.

[46] Vallée T, Keller T, Fourestey G, Fournier B, Correia JR. Adhesively bonded joints composed of pultruded adherends: Considerations at the upper tail of the material strength statistical distribution. Probab Eng Mech 2009;24(3):358–66. http://dx.doi.org/10.1016/j.probengmech.2008.10.001.

[47] Tannert T, Vallée T, Hehl S. Probabilistic strength prediction of adhesively bonded timber joints. Wood Sci Technol 2012;46(1–3):503–13. http://dx.doi.org/10.1007/s00226-011-0424-0.